Research Article Vol. 31, No. 18 / 28 Aug 2023 / Optics Express 29877
Optics EXPRESS

Ultra-broadband 3-dB coupler based on dual-hollow-core polymer fiber covering E + S + C + L + U band

HAOQIANG JIA,[1] SHUQIN LOU,[1] DONGLIAN HOU,[1] LU XUE,[2] XINZHI SHENG,[2] PAUL K CHU,[3] AND XIN WANG[1,*]

[1]*Key Laboratory of Communication and Information Systems, Beijing Municipal Commission of Education, School of Electronic and Information Engineering, Beijing Jiaotong University, Beijing, 100044, China*
[2]*School of Physical Science and Engineering, Beijinssg Jiaotong University, Beijing, 100044, China*
[3]*Department of Physics, Department of Materials Science and Engineering, and Department of Biomedical Engineering, City University of Hong Kong, Kowloon, 999077, China*
[*]*xin.wang@bjtu.edu.cn*

Abstract: An ultra-broadband 3-dB coupler based on a polymer dual-hollow-core anti-resonant fiber (DHC-ARF) is designed to work in the E + S + C + L + U communication band. By incorporating two elliptical-like cores and modulating the air gap between the two cores, the wavelength and polarization dependence of the DHC-ARF-based coupler is reduced effectively. The feasibility of using a 1.46 cm long DHC-ARF as the ultra-broadband coupler for the operating bandwidth of 400 nm in the range between 1.33 μm and 1.73 μm is demonstrated theoretically. The coupling ratio of each polarized mode stabilizes at 50 ± 2% and the coupling ratio difference between the two polarized modes changes within ±0.6%. This DHC-ARF coupler which is made of a polymer can be fabricated by high-resolution 3D printing. Compared to a silica-based DHC-ARF coupler, the polymer-based DHC-ARF coupler is easier to manufacture and the total loss of the latter is only 0.041 ± 0.006 dB in the operating bandwidth. The polymer hollow-core fiber coupler boasting an ultra-broadband, short component length, and low loss is very promising in next-generation, high-speed, and large-capacity hollow-core fiber communication systems.

1. Introduction

Hollow-core fibers (HCFs) have attracted a lot of attention due to their unique properties such as low latency, extremely low nonlinearity, near-zero dispersion, temperature insensitivity, as well as high materials damage threshold [1]. Recent technological advances and new knowledge about the low loss and broadband characteristics of HCFs suggest that they are promising in future ultrawide-bandwidth, high-speed, and low-latency data communications [2,3]. However, the lack of adaptable couplers makes it difficult to exploit the advantages of HCFs in telecommunication systems [4] and therefore, the development of fiber-based couplers adaptable to HCF-based systems is crucial [5].

Since dual-core fiber components are compact and have broadband and high coupling efficiency compared with components composed of lenses, prisms, gratings, and silicon wire waveguides, they are widely used in fiber-based couplers [6–8]. For example, Lee et al. have fabricated a 3-dB fiber coupler based on a dual-core photonic crystal fiber (PCF) [9]. However, the 3-dB coupler can only be operated at 1,550 nm because it is difficult to reduce the wavelength dependence. To widen the operating band of couplers, Laegsgaard et al. have proposed a dual-core PCF coupler by introducing fluorine-doped cores to reduce the wavelength dependence and achieve a broad bandwidth of 0.75 μm [10], but the fluorine-doped cores introduce polarization dependence to the coupler. Suppression of the wavelength dependence as well as polarization dependence is critical to the development of broadband dual-core fiber couplers [11–13]. Most notably, these

#494281 https://doi.org/10.1364/OE.494281
Journal © 2023 Received 27 Apr 2023; revised 14 Jul 2023; accepted 11 Aug 2023; published 24 Aug 2023

Optics EXPRESS

aforementioned couplers consist of solid-core fibers with large Fresnel reflection (>3.5%) at the silica-air interface when the solid-core fiber couplers are spliced into the HCF-based systems [14]. In this respect, a coupler based on the dual-hollow-core fiber (DHCF) is more desirable. However, abatement of the wavelength and polarization dependence for DHCF-based couplers is challenging. Huang et al. have fabricated a dual-hollow-core anti-resonant fiber (DHC-ARF) coupler and demonstrated experimentally that the polarization dependence can be reduced [15]. Because the mode coupling in DHC-ARF is more difficult than that in the dual-solid-core fiber caused by the strong inhabitation of cladding in the DHC-ARF on the mode coupling between the two cores [16], the component length of the fabricated DHC-ARF-based coupler is as large as 40 cm. It is noted that research of DHCF-based couplers is still in the beginning stage [15–20]. There is still a long way to go in the development of HCF-based couplers that can be used in broadband, large-capacity, and low-latency HCF-based systems.

Herein, an ultra-broadband HCF coupler based on a DHC-ARF is designed and analyzed. By modulating the air gap between the two cores and shape of the two cores, the wavelength dependence and polarization dependence of the DHC-ARF-based coupler can be reduced with a short component length. Simulation shows that the 1.46 cm long DHC-ARF is suitable for the broadband HCF coupler with an operating bandwidth of 400 nm in the wavelength range from 1.33 μm to 1.73 μm, thus covering the E + S + C + L + U telecommunication bands. In this operating bandwidth, the coupling ratio (CR) stabilizes at 50 ± 2% and the coupling ratio difference (CRD) varies within ±0.6%. More importantly, the coupler is constructed with a polymer thereby making the coupler easy to produce by high-resolution 3D printing compared to silica HCF-based couplers. The total loss is only 0.041 ± 0.006 dB in the operating bandwidth, suggesting that this polymer HCF coupler with an ultra-broadband, short component length, and low loss has large commercial potential in next-generation high-speed and large-capacity HCF communication systems.

2. Structure and principle

The cross-section of the polymer DHC-ARF is depicted in Fig. 1. The two elliptical-like cores are surrounded by four kinds of circular tubes with diameters of d_g, d_x, d_y, and d_s and a wall thickness of $t = 0.5$ μm to ensure a wide transmission band. An air gap with a width of g is placed between the two hollow cores to form the mode coupling channel for transverse power transfer between the two cores. The two elliptical-like cores and air gap are the key to the wavelength dependence and polarization dependence of the fiber. The host material (represented by blue color) is the polymer IP-Dip and the refractive index is determined by [21]

$$n = \sqrt{1 + \frac{A_1\lambda^2}{\lambda^2 - B_1} + \frac{A_2\lambda^2}{\lambda^2 - B_2} + \frac{A_3\lambda^2}{\lambda^2 - B_3}} \tag{1}$$

where $A_1 = 1.2899$, $A_2 = 6.0569 \times 10^{-2}$, $A_3 = 1.1844 \times 10^5$, $B_1 = 1.1283 \times 10^{-2}$ μm^2, $B_2 = 7.7762 \times 10^{-2}$ μm^2, $B_3 = 2.5802 \times 10^7$ μm^2, and λ is the wavelength.

According to the coupled-mode theory, there are four fundamental supermodes in the DHC-ARF, namely the y-polarized (y-pol) odd mode, y-pol even mode, x-polarized (x-pol) odd mode, and x-pol even mode, as shown in Fig. 2(a). The coupling length (L_c), a key parameter to evaluate the coupling performance, is defined as the transmission length over which the light power in one core can be transferred completely to the other core, and can be expressed as follows:

$$L_c^{y(x)} = \lambda/2|\Delta n^{y(x)}| \tag{2}$$

where $L_c^{y(x)}$ is the coupling length L_c of the x or y-pol mode, $\Delta_n y(x)$ denotes the difference of the effective refractive index between a pair of y-pol supermodes (n_o^y and n_e^y) or x-pol supermodes (n_o^x and n_e^x).

Optics EXPRESS

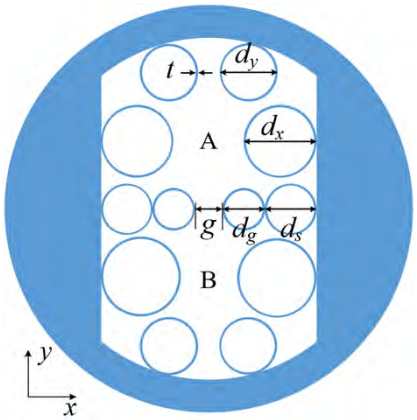

Fig. 1. Cross-section of the polymer DHC-ARF.

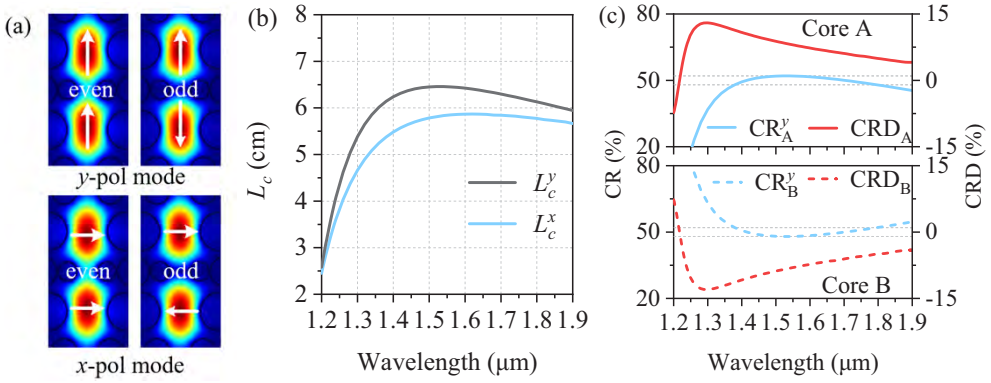

Fig. 2. Modal fields of the four fundamental supermodes at 1550 nm (a), variations of L_c of the DHC-ARF (b), and variations of CR_A^y and CRD_A of the DHC-ARF-based coupler (c).

To design a broadband, high-performance broadband 3-dB coupler based on the dual-core fiber, L_c^y and L_c^x of the fiber should remain unchanged and be nearly equal throughout the transmission window. Smaller wavelength dependence and polarization dependence of DCH-ARF is the key challenge in designing the 3-dB coupler. CR and CRD are usually utilized to evaluate the wavelength dependence of a coupler. CR represents the power ratio of one polarized mode at the two output ends of a coupler and CRD is the difference of the CR between two polarized modes at the one output of a coupler. Generally, for a 3-dB coupler in optical communication systems, the CR of the coupler is expected to be in the range of 48% to 52% and the CRD of a coupler is expected to be within ±1%. CR and CRD can be expressed as [12]:

$$\mathrm{CR}_{\mathrm{A}}^{y(x)} : \mathrm{CR}_{\mathrm{B}}^{y(x)} = P_{\mathrm{A}}^{y(x)}/(P_{\mathrm{A}}^{y(x)} + P_{\mathrm{B}}^{y(x)}) \times 100\% : P_{\mathrm{B}}^{y(x)}/(P_{\mathrm{A}}^{y(x)} + P_{\mathrm{B}}^{y(x)}) \times 100\% \tag{3}$$

$$\mathrm{CRD}_{\mathrm{A(B)}} = \mathrm{CR}_{\mathrm{A(B)}}^{y} - \mathrm{CR}_{\mathrm{A(B)}}^{x} \tag{4}$$

where $\mathrm{CR}_{\mathrm{A}}^{y(x)}$ is the CR of the $y(x)$-pol mode in core A, $\mathrm{CR}_{\mathrm{B}}^{y(x)}$ is the CR of the $y(x)$-pol mode in core B, $\mathrm{CRD}_{\mathrm{A(B)}}$ denotes the difference in the CR between the two polarized modes in core A(B), $P_{\mathrm{A}}^{y(x)}$ is the output power of the $y(x)$-pol mode in core A, and $P_{\mathrm{B}}^{y(x)}$ is the output power of

Optics EXPRESS

the $y(x)$-pol mode in core B which can be calculated by [12]:

$$P_{\mathrm{A}}^{y(x)} = P_0^{y(x)} \cos^2(\pi L / 2L_{\mathrm{c}}^{y(x)}) \tag{5}$$

$$P_{\mathrm{B}}^{y(x)} = P_0^{y(x)} - P_{\mathrm{A}}^{y(x)} \tag{6}$$

$$L = 2 \max(L_{\mathrm{c}}^{y}, L_{\mathrm{c}}^{x}) \arccos(\sqrt{0.52})/\pi \tag{7}$$

where $P_0^{y(x)}$ is the normalized input power of the $y(x)$-pol mode in core A, L is the component length of the coupler with CR stablized at $50 \pm 2\%$, and $\max(L_c^y, L_c^x)$ is the maximum value between L_c^y and L_c^x in the first anti-resonant window.

Figure 2 shows the results of the DHC-ARF obtained by the finite element method in which a perfectly matched layer is implemented to accurately calculate the modal characteristics of the fiber by adopting extremely fine meshes of $\lambda/6$, $\lambda/4$, and $\lambda/4$ in the polymer regions, air regions, and perfectly matched layer, respectively. For $g = 8.5$ µm, $d_g = 13$ µm, $d_x = 18$ µm, $d_y = 12$ µm, $d_s = 9.75$ µm, and $t = 0.5$ µm, the modal fields of the fundamental modes at 1,550 nm are shown in Fig. 2(a) and the corresponding L_c at 1,550 nm can be calculated by Eq. (2). By simulating the modal characteristics at different wavelengths, the variations of L_c with wavelength are derived and Fig. 2(b) shows that L_c is only several centimeters, while the L_c^y and L_c^x curves exhibit a similar trend between 1.2 µm and 1.9 µm. To determine the broadband characteristics of the coupler, L_c of the fiber should maintain a flat variation trend over a wide bandwidth. In the wavelength range from 1.38 µm to 1.8 µm, L_c about 6 cm is conducive to obtaining the broadband coupler. However, there is a difference between L_c^y and L_c^x, which results in a significant polarization dependence and degrades the broadband characteristics of the coupler. For example, and L_c^x are 5.84 cm and 6.45 cm at 1,550 nm, respectively. Although the difference between L_c^y and is only 0.61 cm, an evident polarization dependence is observed from the DHC-ARF-based coupler. As shown in Fig. 2(c), when a 3.14 cm long fiber is used, the CR of the y-pol mode in core A and core B ($\mathrm{CR_A^y}$ and $\mathrm{CR_B^y}$) is $50 \pm 2\%$ from 1.38 µm to 1.8 µm, but the CRD in core A ($\mathrm{CRD_A}$) is as high as 8.02% at 1,550 nm and CRD in core B ($\mathrm{CRD_B}$) is as low as -8.02%. Hence, it is necessary to reduce the wavelength dependence and polarization dependence of a coupler simultaneously.

3. Wavelength and polarization dependence

The effects of the structural parameters on the wavelength dependence and polarization dependence are analyzed. The air gap region formed by an air gap (width of g) and cladding tubes (diameters of d_g and d_s) serves as a mode-coupling channel between the two hollow cores and plays an important role in the wavelength dependence. Firstly, the effects of g are analyzed by changing d_s. Figure 3 shows the variations of the coupling ratio and component length (CR and L) with g. When g is varied from 7 µm to 12 µm while d_g is fixed at 8 µm (d_s changing from 15.5 µm to 13 µm), Fig. 3(a) shows that $\mathrm{CR_A^y}$ is stable at $50 \pm 2\%$ in the wavelength ranges from 1.426 µm to 1.917 µm, from 1.375 µm to 1.829 µm, from 1.33 µm to 1.73 µm, from 1.293 µm to 1.639 µm, from 1.257 µm to 1.56 µm, and 1.216 µm to 1.488 µm, respectively. The corresponding bandwidth decreases from 491 nm to 272 nm because a larger g enhances mode coupling between the two cores, especially at short wavelengths as the coupler is close to the resonant wavelength. It seems difficult to reduce the wavelength dependence at short wavelengths and thus the $\mathrm{CR_A^y}$ curve shows a rapid decline at short wavelengths. When g is reduced, the mode coupling between the two cores weakens, especially at long wavelengths. A smaller g abates the wavelength dependence at longer wavelengths and widens the bandwidth. The variation of the component length L is shown in Fig. 3(b). When g increases from 7 µm to 12 µm, L decreases from 3.57 cm to 0.56 cm. As shown by the modal fields in the insets in Fig. 3(b), when g increases, the electric field strength increases in the air gap, indicating that a larger g enhances the mode coupling between the two cores and L_c can thus be reduced. Since L is proportional to L_c, L can be reduced by increasing

Optics EXPRESS

g. However, to improve the broadband characteristics of the coupler, a narrow air gap width g should be selected.

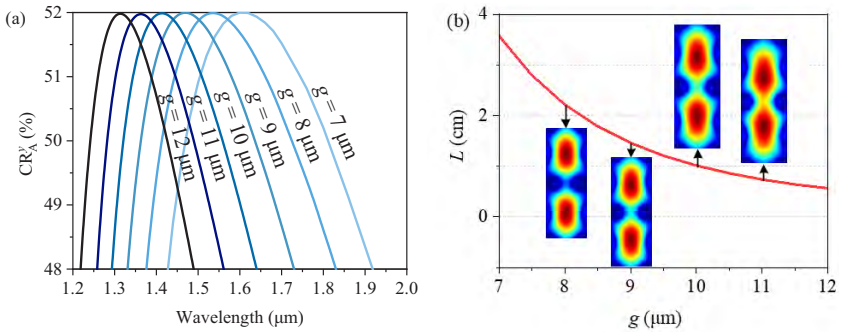

Fig. 3. Impact of g on CR (a) and L (b).

The impact of d_g is assessed by changing d_s. Figure 4 shows the variation of CR and L with d_g, when d_g increases from 4 μm to 12 μm while g is fixed at 9 μm (d_s decreasing from 18.5 μm to 12.5 μm). Figure 4(a) shows that the wavelength range where CR stabilizes within 50 ± 2% shifts to long wavelengths, while the wavelength region is almost unchanged when d_g changes from 8 μm to 12 μm. When d_g increases from 4 μm to 12 μm, the corresponding bandwidth increases from 396 nm to 400 nm and then decreases to 393 nm. The variation of d_g shows a small effect on the wavelength dependence. The variation of L with d_g is presented in Fig. 4(b). When d_g increases from 4 μm to 12 μm, L increases from 1.05 cm to 2.24 cm. The electric field strength in the insets in Fig. 4(b) show that mode coupling between the two cores weakens with increasing d_g and hence, a large d_g results in a large L. Meanwhile, when d_g is varied from 4 μm to 12 μm, d_g has only a small impact on the wavelength dependence of the coupler.

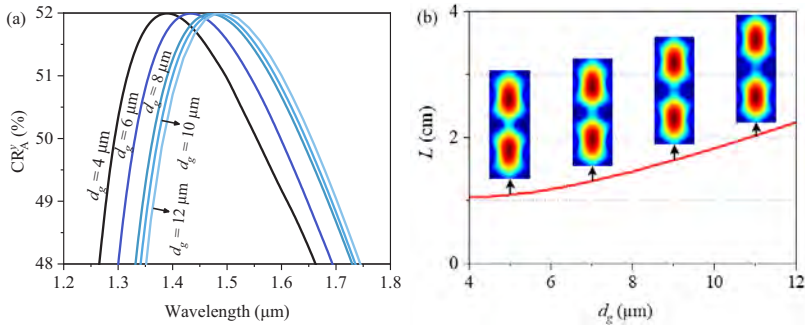

Fig. 4. Impact of d_g on CR (a) and L (b).

The wavelength dependence of the DHC-ARF-based coupler is also affected by the shape of the two cores in the fiber. Because the elliptical-like cores are impacted by the diameter of cladding tubes (d_x), the effects of the shape of the two cores on the wavelength dependence of coupler is analyzed under different d_x. Figure 5 shows the variation of CR and L with d_x when d_x increases from 12 μm to 20 μm (core diameter in the x-direction decreasing from 30 μm to 14 μm). Figure 5(a) shows that the wavelength region where CR stabilizes at 50 ± 2% is almost unchanged when d_x changes from 12 μm to 18 μm. When d_x increases from 12 μm to 20 μm, the corresponding bandwidth decreases from 416 nm to 353 nm. A small d_x gives rise to the broadband, but the bandwidth of CR_A^y within 50 ± 2% only increases from 400 nm to 416 nm

Optics EXPRESS

when d_x decreases from 18 μm to 12 μm. The variation of L with d_x is presented in Fig. 5(b). When d_x increases from 12 μm to 20 μm, L decreases from 3.09 cm to 0.81 cm. The insets in Fig. 5(b) show that the electric field strength at the air gap increases when d_x increases, and mode coupling between the two cores is enhanced by increasing d_x. Hence, d_x can be selected between 12 μm and 18 μm in order to reduce the wavelength dependence.

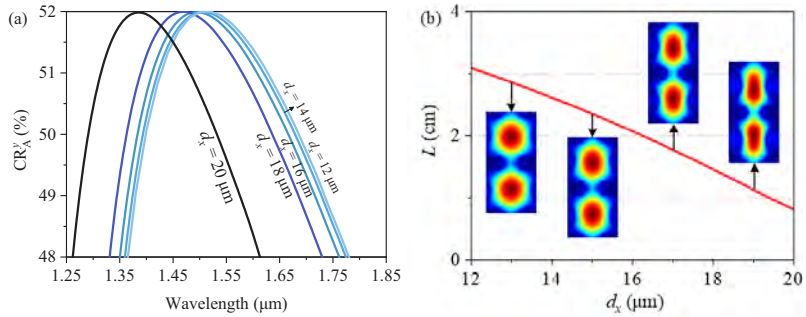

Fig. 5. Impact of d_x on CR (a) and L (b).

According to the above analysis, it is evident that smaller g and d_x mitigate effectively the wavelength dependence of the coupler, while changing d_g has little effects in suppressing the wavelength dependence. Furthermore, analysis of the component length reveals that increasing g or d_x decreases L, while a smaller d_g only decreases L slightly. Since g, d_g, and d_x affect not only the wavelength dependence, but also the polarization dependence, the effects of d_x, g, and d_g on the polarization dependence are analyzed. By adjusting d_x, the elliptical core is formed. When d_x increases from 16 μm to 20 μm, the impact of d_x on the CRD of a coupler is shown in Fig. 6(a). The grey region indicates CRD_A stabilization within ±1%. When d_x changes from 16 μm to 17 μm and then 18 μm, the wavelength region in which CRD_A stabilizes within ±1% spans the regions from 1,655 nm to 1,900 nm, from 1,250 nm to 1,282 nm and from 1,578 nm to 1,880 nm, and from 1,292 nm to 1,796 nm. CRD_A depends strongly on d_x. When d_x is 18 μm, the polarization dependence weakens, and the wavelength region where CRD_A stabilizes within ±1% covers the E + S + C + L + U band.

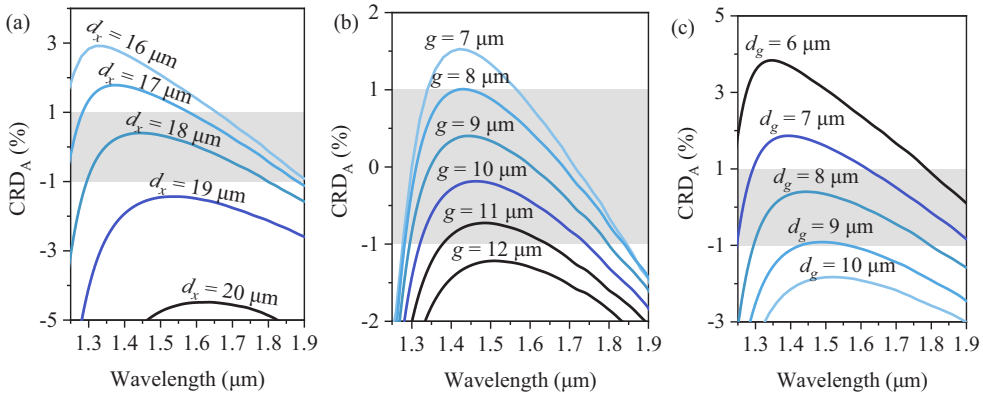

Fig. 6. Impact of d_x (a), g (b), and d_g (c) on CRD.

Next, the impacts of g and d_g are analyzed as shown in Figs. 6(b) and 6(c). When g increases from 7 μm to 12 μm, Fig. 6(b) shows that CRD_A decreases with increasing g. When g changes from 7 μm, 8 μm, 9 μm, 10 μm to 11 μm, the wavelength region where CRD_A stabilizes within

Optics EXPRESS

±1% covers the ranges from 1,277 nm to 1,340 nm and from 1,566 nm to 1,845 nm, from 1,281 nm to 1,409 nm and from 1,455 nm to 1,838 nm, from 1,292 nm to 1,796 nm, from 1,319 nm to 1,741 nm, and from 1,376 nm to 1,641 nm. For $g = 9$ μm or 10 μm, the wavelength region in which CRD_A stabilizes at ±1% covers the E + S + C + L + U band. To obtain the widest wavelength region, $g = 9$ μm is selected. When d_g increases from 6 μm to 10 μm, Fig. 6(c) shows that CRD_A decreases with increasing d_g. When $d_g = 8$ μm, the wavelength region in which CRD_A stabilizes within ±1% spans the range between 1,292 nm and 1,796 nm for the E + S + C + L + U band.

Besides, we also analyze the impact of d_y on the CR, CRD and L of a coupler, and conclude that the d_y shows a little influence on the coupler compared to g, d_g, and d_x. To reduce the polarization dependence of the coupler, precise modulation of the cladding tube diameter d_x is crucial in addition to d_g, compared to g. Therefore, g, d_g, and d_x are set to 9 μm, 8 μm and 18 μm, while d_y and d_s are 12 μm and 14.5 μm, respectively.

4. Properties of 3-dB coupler based on polymer DHC-ARF

When a 1.46 cm long DHC-ARF are used as a coupler, the properties of the coupler are determined at 1,550 nm firstly. When light is coupled into core A and propagates by 3 cm, Fig. 7 shows that the CR curves of the two polarized modes exhibit the same variation trend in core A or core B, in which $CR_A^{y,x}$ decreases and $CR_B^{y,x}$ increases with propagation distance. When the two polarized modes propagate after a distance L of 1.46 cm, CR_A^y, CR_A^x and CRD_A are 51.43%, 51.22%, and 0.21%, while CR_B^y, CR_B^x and CRD_B are 48.57%, 48.78% and -0.21%, respectively. Therefore, at the two outputs of the coupler, CR remains at 50 ± 2% and CRD stabilizes to within ± 1% at 1,550 nm, providing evidence that the 3-dB coupler based on the 1.46 cm long DHC-ARF can be implemented at 1,550 nm.

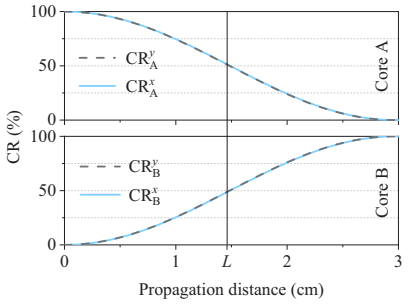

Fig. 7. Variation of $CR_A^{y,x}$ and with propagation distance at 1,550 nm.

The properties of the coupler are determined between 1.25 μm and 1.85 μm, as shown in Fig. 8. In core A, CR_A^y rises from 48% to 52% and then decreases to 48% from 1.33 μm to 1.73 μm. CR_A^x increases initially from 48% to 51.61% and then decreases to 48% from 1.328 μm to 1.762 μm, while CRD_A rises from -1% to 0.41% and then decreases to -1% from 1.294 μm to 1.796 μm. In core B, CR_B^y decreases from 52% to 48% initially and then increases to 52% from 1.33 μm to 1.73 μm, while CR_B^x decreases from 52% to 48.39% and increases to 52% from 1.328 μm to 1.762 μm. CRD_B decreases from 1% to -0.41% and then rises to 1% from 1.294 μm to 1.796 μm. The results show that $CR_A^{y,x}$ can be stablized at 50 ± 2%, while CRD is within ±1% in the wavelength range between 1.33 μm and 1.73 μm. Hence, a broadband coupler with a bandwidth of 400 nm can be developed with the aid of the 1.46 cm long polymer DHC-ARF.

The loss of the coupler is evaluated. The component loss is mainly determined by the total loss of the DHC-ARF and the component length. The total loss of the polymer DHC-ARF includes

Optics EXPRESS

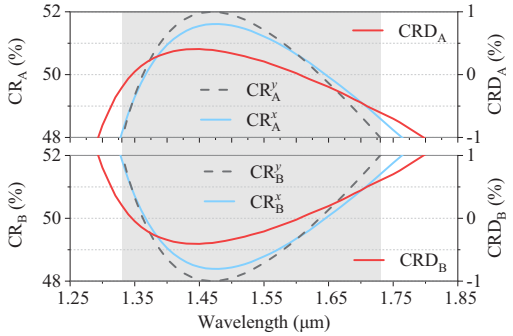

Fig. 8. Properties of the 3-dB coupler in the wavelength range between 1.25 μm and 1.85 μm.

primarily the confinement loss (CL) and absorption loss (α) as shown below:

$$\mathrm{CL} = 8.686 k_0 \mathrm{Im}(n_{eff}) \ [\mathrm{dB/m}] \tag{8}$$

$$\alpha = \frac{\int_{polymer} \alpha_{\mathrm{mat}} n \sqrt{\varepsilon_0/\mu_0} |E|^2 dA}{\mathrm{Re}\left\{\hat{z} \cdot \int_{all} E \times H^* dA\right\}} \ [\mathrm{dB/m}] \tag{9}$$

where $k_0 = 2\pi/\lambda$ is the wave vector, λ is the wavelength, $\mathrm{Im}(n_{eff})$ represents the imaginary part of the n_{eff}; α_{mat} is the absorption coefficient of the materials [21], n is the refractive index of the polymer IP-Dip, ε_0 and μ_0 are the dielectric constant and magnetic permeability in a vacuum, respectively, E and H are the electric field and magnetic field components, respectively. Integration of the numerator is performed over the region of the polymer and that of the denominator is carried out over all the fiber regions.

The total loss, α and CL of the polymer DHC-ARF, and the CL of a silica DHC-ARF are shown in Fig. 9. Between 1.33 μm and 1.73 μm, the total loss of the polymer varies from 0.024 dB/cm to 0.032 dB/cm the α changes from 0.0019 dB/cm to 0.0083 dB/cm and the CL of the polymer DHC-ARF varies from 0.021 dB/cm to 0.027 dB/cm, whereas the CL of the silica DHC-ARF varies from 0.017 dB/cm to 0.023 dB/cm. At 1,550 nm, the total loss of the polymer DHC-ARF, CL of the polymer DHC-ARF, and CL of the silica DHC-ARF are 0.024 dB/cm, 0.021 dB/cm and 0.019 dB/cm, respectively. The total loss of the polymer DHC-ARF is low and mainly depends on the CL of the polymer DHC-ARF. The CL of the polymer fiber is comparable to that of silica DHC-ARF. The component loss of the coupler based on the 1.46 cm long polymer DHC-ARF is obtained by multiplying the total loss of the fiber with the length of 1.46 cm. The loss of the coupler ranges from 0.035 dB to 0.047 dB between 1.33 μm and 1.73 μm and the broadband coupler shows a low loss of 0.041 ± 0.006 dB in the operating band.

Finally, the tolerance of the coupler is assessed. It is important to precisely control the transverse geometry of the dual-core fiber during manufacturing. Although Bertoncini et al. [22] have fabricated IP-Dip-based HCFs with complex claddings by high-precision 3D printing, fabrication of three-dimensional nanoscale structures is still challenging. The thickness of the cladding tubes t has a nanoscale and t is a key guiding characteristic of the DHC-ARF. Hence, the tolerance of t is assessed by setting the variation of t as ηt. The impact of η_t on the characteristics of the coupler constructed with the 1.46 cm long polymer DHC-ARF is presented in Fig. 10. The white solid line and solid line represent $\mathrm{CR}_\mathrm{A}^\mathrm{y} = 48\%$ and $\mathrm{CR}_\mathrm{A}^\mathrm{y} = 52\%$, the black dot line represents $\mathrm{CRD_A} = -1\%$, and the dashed area indicates the E + S + C + L + U band. Stabilized CR (50 ± 2%) has a lower tolerance for t than CRD within ±1% and therefore, is mainly determined

Optics EXPRESS

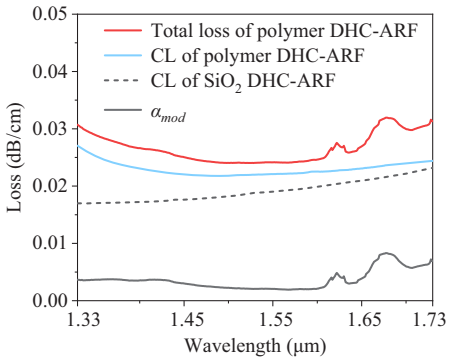

Fig. 9. Loss of the DHC-ARF.

by CR. For η_t in the range between 0% and 1%, the two red lines in Fig. 10(a) shows that the operating bandwidth of a coupler covers the E + S + C + L + U band.

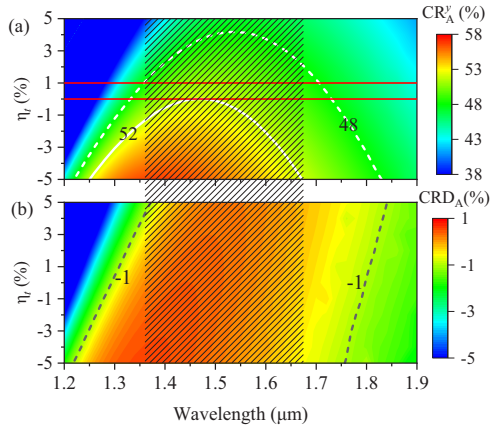

Fig. 10. Impact of on (a) and CRD_A (b) of a coupler.

5. Conclusion

An ultra-broadband HCF coupler based on a polymer DHC-ARF is first designed and analyzed. Adjusting the air gap g and tube diameter d_x weakens the wavelength dependence, and the polarization dependence of the fiber can be reduced by changing the tube diameters d_x and d_g. The simulation results show the broadband coupler comprising a 1.46 cm long DHC-ARF has an operating bandwidth of 400 nm covering wavelengths between 1.33 μm to 1.73 μm, in which range CR is stabilized at 50 ± 2% and CRD ranges within ±0.6%. Although the DHC-ARF-based coupler is made of a polymer, the component loss remains low at 0.041 ± 0.006 dB in the operating bandwidth. This 3-dB HCF coupler with an ultra-broadband, short component length, and low loss has immense potential in next-generation, high-speed, and large-capacity HCF communication systems.

Funding. National Natural Science Foundation of China (12174022); Beijing Municipal Natural Science Foundation (1232028).

Disclosures. The authors declare that there are no conflicts of interest related to this article.

Optics EXPRESS

Data availability. Data underlying the results presented in this paper are not publicly available at this time but may be obtained from the authors upon reasonable request.

References

1. C. Wei, R. Joseph Weiblen, C. R. Menyuk, and J. Hu, "Negative curvature fibers," Adv. Opt. Photon. **9**(3), 504–561 (2017).
2. H. Sakr, Y. Hong, T. D. Bradley, G. T. Jasion, J. R. Hayes, H. Kim, I. A. Davidson, E. N. Fokoua, Y. Chen, K. R. H. Bottrill, N. Taengnoi, N. V. Wheeler, P. Petropoulos, D. J. Richardson, and F. Poletti, "Interband short reach data transmission in ultrawide bandwidth hollow core fiber," J. Lightwave Technol. **38**(1), 159–165 (2020).
3. G. T. Jasion, H. Sakr, J. R. Hayes, S. R. Sandoghchi, L. Hooper, E. N. Fokoua, A. Saljoghei, H. C. Mulvad, M. Alonso, A. Taranta, T. D. Bradley, I. A. Davidson, Y. Chen, D. J. Richardson, and F. Poletti, "0.174 dB/km hollow core double nested antiresonant nodeless fiber (DNANF)," in *2022 Optical Fiber Communications Conference and Exhibition*, 1–3 (2022).
4. Y. Jung, H. Kim, Y. Chen, T. D. Bradley, I. A. Davidson, J. R. Hayes, G. Jasion, H. Sakr, S. Rikimi, F. Poletti, and D. J. Richardson, "Compact micro-optic based components for hollow core fibers," Opt. Express **28**(2), 1518–1525 (2020).
5. X. Suo, H. Yu, J. Li, and X. Wu, "Transmissive resonant fiber-optic gyroscope employing Kagome hollow-core photonic crystal fiber resonator," Opt. Lett. **45**(8), 2227–2230 (2020).
6. D. Drolet and R. Vallée, "Dual-core fiber as a tunable directional coupler," Opt. Lett. **18**(6), 408–410 (1993).
7. H. Jiang, E. Wang, J. Zhang, L. Hu, Q. Mao, Q. Li, and K. Xie, "Polarization splitter based on dual-core photonic crystal fiber," Opt. Express **22**(25), 30461–30466 (2014).
8. T. Joseph and J. John, "Two-core fiber-based mode converter and mode demultiplexer," J. Opt. Soc. Am. B **36**(8), 1987–1994 (2019).
9. B. H. Lee, J. B. Eom, J. Kim, D. S. Moon, U.-C. Paek, and G.-H. Yang, "Photonic crystal fiber coupler," Opt. Lett. **27**(10), 812–814 (2002).
10. J. Laegsgaard, O. Bang, and A. Bjarklev, "Photonic crystal fiber design for broadband directional coupling," Opt. Lett. **29**(21), 2473–2475 (2004).
11. S. K. Varshney, N. J. Florous, K. Saitoh, and M. Koshiba, "The impact of elliptical deformations for optimizing the performance of dual-core fluorine-doped photonic crystal fiber couplers," Opt. Express **14**(5), 1982–1995 (2006).
12. S. Lou, Z. Tang, and L. Wang, "Design and optimization of broadband and polarization-insensitive dual-core photonic crystal fiber coupler," Appl. Opt. **50**(14), 2016–2023 (2011).
13. T. Zhao, S. Lou, X. Wang, M. Zhou, and Z. Lian, "Ultrabroadband polarization-insensitive coupler based on dual-core photonic crystal fiber," IEEE Photonics J. **9**(1), 1–10 (2017).
14. F. Couny, F. Benabid, and P. S. Light, "Reduction of Fresnel back-reflection at splice interface between hollow core PCF and single-mode fiber," IEEE Photon. Technol. Lett. **19**(13), 1020–1022 (2007).
15. X. Huang, J. Ma, D. Tang, and S. Yoo, "Hollow-core air-gap anti-resonant fiber couplers," Opt. Express **25**(23), 29296–29306 (2017).
16. A. Argyros, S. G. Leon-Saval, and M. A. van Eijkelenborg, "Twin-hollow-core optical fibres," Opt. Commun. **282**(9), 1785–1788 (2009).
17. N. Wheeler, T. Bradley, J. Hayes, G. Jasion, Y. Chen, S. Sandoghchi, P. Horak, F. Poletti, M. Petrovich, and D. Richardson, "Dual hollow-core anti-resonant fibres," SPIE Photonics Europe **9886**, 988617 (2016).
18. X. Liu, Z. Fan, Z. Shi, Y. Ma, J. Yu, and J. Zhang, "Dual-core antiresonant hollow core fibers," Opt. Express **24**(15), 17453–17458 (2016).
19. H. Jia, X. Wang, S. Gu, and S. Lou, "Decoupling of dual-hollow-core anti-resonant fiber," Optik **273**, 170495 (2023).
20. H. Jia, X. Wang, B. Huang, L. Xue, X. Sheng, and S. Lou, "Compact single-polarization coupler based on a dual-hollow-core anti-resonant fiber," Opt. Express **31**(8), 12410–12422 (2023).
21. M. Schmid, D. Ludescher, and H. Giessen, "Optical properties of photoresists for femtosecond 3D printing: refractive index, extinction, luminescence-dose dependence, aging, heat treatment and comparison between 1-photon and 2-photon exposure," Opt. Mater. Express **9**(12), 4564–4577 (2019).
22. A. Bertoncini and C. Liberale, "3D printed waveguides based on photonic crystal fiber designs for complex fiber-end photonic devices," Optica **7**(11), 1487–1494 (2020).